Comparison of the Flow Properties of Rocks at Crustal Conditions

H. C. Heard

Email alerting service	Receive free email alerts when new articles cite this article - sign up in the box at the top right-hand corner of the article or click **here**

Comparison of the flow properties of rocks at crustal conditions

By H. C. Heard

Lawrence Livermore Laboratory, University of California, Livermore,
California 94550, U.S.A.

It is inferred that, although both primary and tertiary creep may be important in certain regions, large-scale ductile deformation in the Earth's crust must be governed by secondary creep (steady state). This flow involves plastic deformation resulting from dislocation motion and diffusion. Geological, geophysical and geochemical observations constrain the temperature (T), strain rate ($\dot{\epsilon}$), and stress difference (σ) for rocks undergoing secondary creep to: -30–800 °C, 10^{-7}–10^{-15} s^{-1}, and up to 300 MPa (3 kbar). The actual conditions of secondary creep are strongly dependent on rock type and depth of deformation.

Useful laboratory data on rocks obtained over wide ranges of T, $\dot{\epsilon}$ and σ are limited to ice, halite, marble, dolomite, quartzite and dunite. Steady-state flow results are available for both wet and dry rocks; H_2O strongly affects the behaviour of both quartzite and dunite, but has a negligible effect on halite and marble. Secondary creep data for each rock are well fitted by $\dot{\epsilon} = A \exp(-Q/RT)\,\sigma^n$, where Q is an activation energy for creep (diffusion) and A, R, n are constants.

Comparison between those rocks expected in the deep crust indicates that at the highest T and at $\dot{\epsilon}$ of 10^{-12}–10^{-15} s^{-1}, σ is largest for dry dunite and dolomite, followed by dry quartzite, marble and wet quartzite. Equivalent viscosities (η) range from 10^{18}–10^{22} Pa s (10^{19}–10^{23} P). At intermediate depths (at $T = 300$–500 °C), σ in dolomite is slightly greater than dry quartzite; both are much stronger than marble. In the shallow crust, secondary creep is expected only in marble ($T > 250$ °C) and in halite ($T > 25$ °C). The η of halite at 25–250 °C, range from 10^{21}–10^{17} Pa s. At the surface and at $\dot{\epsilon}$ of 10^{-7}–10^{-10} s^{-1} (glacier flow), η of ice would be 10^{15} to 10^{12} Pa s between -30 and 0 °C. Values of η for all rocks examined appear insensitive to T except wet quartzite and all dunite.

Introduction

The mechanical behaviour of rocks indigenous to the Earth's crust as well as those deformation mechanisms contributing to this behaviour have been shown to be controlled by the tectonic environment during the period of deformation. This observation is based upon laboratory studies accomplished primarily since 1900 taken together with limited field data on the natural deformation environment at depth. Only indirectly may we infer the actual physical/chemical conditions under which a crustal rock was deformed; all direct data on the deformational behaviour of rock have come from tests made in the laboratory at controlled conditions.

Among the environmental parameters affecting rock behaviour are: pressure, temperature, pore fluid pressure, deviatoric stress field, deformation rate and chemical environment. Properties of the rock or component minerals contributing to the overall response include: grain size, mineral composition, degree of order, state of imperfection, homogeneity, anisotropy, porosity, permeability, and intergranular cement. With the exception of chemical effects, the influence of the former group of rock properties on brittle behaviour has been documented elsewhere (Heard 1967).

The purpose of this paper is to emphasize the ductile flow characteristics of rocks as limited by the conditions thought to occur commonly in the crust. We will first attempt to set reasonable limits on the flow environment in the continental crust, then extrapolate available laboratory data characterizing a group of common rocks to those conditions, and finally to compare the deduced flow properties occurring during natural deformation.

CRUSTAL ENVIRONMENT, MECHANICAL RESPONSE AND DEFORMATION MECHANISMS

Crustal temperatures may be estimated from borehole temperatures and heat flow observations, coupled with thermal conductivity measurements and indirect evidence suggesting the chemical composition of the rocks at depth. In thick sedimentary basins in the continental crust such as the U.S. Gulf Coast, thermal gradients range from about 22 °C km^{-1} for offshore Louisiana to about 36 °C km^{-1} for onshore Texas (Nichols 1947; Moses 1961; Gretener 1967).
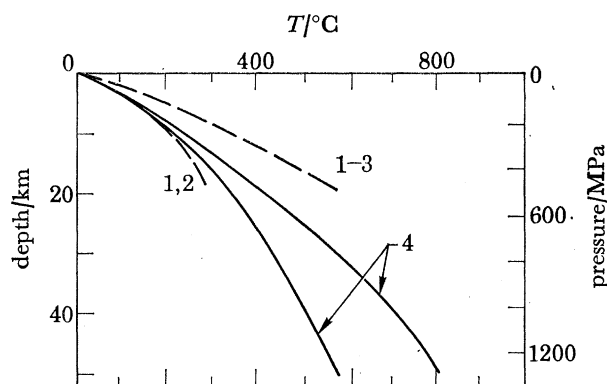

FIGURE 1. Inferred maximum and minimum probable temperatures against depth for continental crust. 1, Nichols (1947); 2, Moses (1961); 3, Gretener (1967); and 4, Lachenbruch (1968). Pressure scale to 6 km based on density depth for thick sedimentary basins (Dickinson 1953). At depths in excess of 6 km, a constant density of 2.7 g/cm^3 was assumed.

Linear extrapolation of these data to depths encountered in sedimentary basins would lead to widespread melting in shallow regions. No evidence exists for such melting and thus the gradient must decrease with depth (figure 1). Lachenbruch (1968) has calculated temperature against depth for the Sierra Nevada batholith, a thickened region of the crust composed primarily of granodiorites. Figure 1 also shows his maximum and minimum thermal profiles based on borehole data with assumptions about the distribution of radioactive heat sources and on surface observations. Herrin (1972) has calculated crustal temperatures for the Basin and Range provinces as well as the Canadian Shield based on similar data. Where comparisons may be made, maximum and minimum values are similar to those of Lachenbruch, even though the rock types and tectonic regions differ widely. If we assume that these profiles are representative of the continental crust as a whole, then the temperatures that might be expected could extend from ambient values at the surface to 250–450 °C at 15 km; 450–600 °C at 30 km and perhaps 550–800 °C at 50 km. At the surface, temperatures representative of temperate and polar glaciers range between 0 and about −30 °C (Kamb 1964; Gow et al. 1968).

Lithostatic pressures may be calculated from the density and height of the rock column. For

granodioritic terranes, calculated pressures at 15, 30 and 50 km would be about 390, 780 and 1300 MPa (3.9, 7.8 and 13.0 kbar), respectively. Pressures from thick sedimentary basins can be expected to be slightly less and somewhat nonlinear with depth, especially near the surface (Dickinson 1953). Lithostatic pressure values are also related to depth in figure 1.

Pore fluid pressures at depth are strongly dependent upon the fluid density and viscosity, rock permeability, the rate of compaction (or expansion) of the rock as well as any dehydration or reaction of the mineral phases present. Pressures could approach 10^5 Pa near the surface, but in many sedimentary basins, pore pressures at depths to several kilometres can be approximated by the pressure exerted at the base of a water column extending to the surface (Hubbert & Rubey 1959). However, at greater depths, Hubbert & Rubey (1959) and Rubey & Hubbert (1959) present data suggesting that pore fluid pressures in sediments often approach and occasionally are slightly greater than those exerted by the overburden. These local high fluid pressures are presumably the result of lowered rock permeabilities coupled with relatively high compaction rates or to dehydration reactions of hydrous minerals during prograde metamorphism. Few borehole observations are available from crystalline igneous terranes and thus values of pore pressures at depth are largely unknown in these rocks.

Estimates of maximum principal stress differences can be made from surface topography coupled with assumptions as to the crustal response. A calculation by Jeffreys (1970) showed that, for a 1 km surface load (density = 2.5 g cm^{-3}) imposed on a low-density elastic crust floating on a denser substratum, stress differences can reach 300 MPa in the upper crust. If the crust is assumed to be elastic-plastic or if it possesses a discontinuity at the edge of the 1 km load, maximum values are nearer 200 MPa (Birch 1964; Jeffreys 1970). The very large gravity anomalies in Hawaii or in the Indonesian Arc suggest stress differences in the crust of about 200 MPa (Birch 1964). Maximum stress values existing at least locally in the continental crust are therefore taken to be 300 MPa. Minimum stress differences necessary for flow depend not only on the rock type but upon the strain rate and temperature (and perhaps the presence of H_2O) as will be discussed below. Minimum stresses considered for the purpose of this paper are arbitrarily set at 10^2 Pa.

The time available for deformation in the crust is of course limited by the age of the particular rock in question. Estimates of natural strain rates in the crust are based on geodetic measurements from surface strains as along the San Andreas fault (Whitten 1956), from rebound rates associated with crustal unloading (Crittenden 1967), from displacement rates of demonstrated sea floor spreading (Heirtzler et al. 1968; Le Pichon 1973), and from estimated rates of crustal shortening in orogenic regions (Gilluly 1972). Values so estimated generally lie between 10^{-13} and 10^{-14} s^{-1}. Recognizing that local strain rates may differ from these values, limits of 10^{-12}–10^{-15} s^{-1} should encompass nearly all significant flow in the intermediate-deep crust. Measurements of flow in glaciers at the surface yield strain rates of 10^{-7}–10^{-10} s^{-1} (Gerrard et al. 1952; Meier 1960; Paterson & Savage 1963).

Chemical processes such as mineral solution in pore fluids with subsequent redeposition, solid–solid or solid–melt phase reactions (see, for example, Griggs 1940; Bridgeman 1945; Griggs & Handin 1960) can enhance ductility and degrade strength in certain rocks. With the exception of fragmentary data on the effects of trace amounts of H_2O in the structure of silicate minerals making up certain rocks (Griggs & Blacic 1965; Griggs 1967), few data are available on the importance of chemical effects on the expected flow properties of rocks at crustal conditions.

For loading in uniaxial stress, general patterns of rock response to an imposed deviatoric

stress are shown schematically in figure 2 (Griggs & Handin 1960; Heard 1967). In the top row, a rock subjected to compressive loading in the laboratory fails by tensile fracture at low relative values of pressure and temperature and at high values of pore pressure and strain rate. Invariably, these fractures are oriented parallel to the maximum principal stress σ_1. A typical
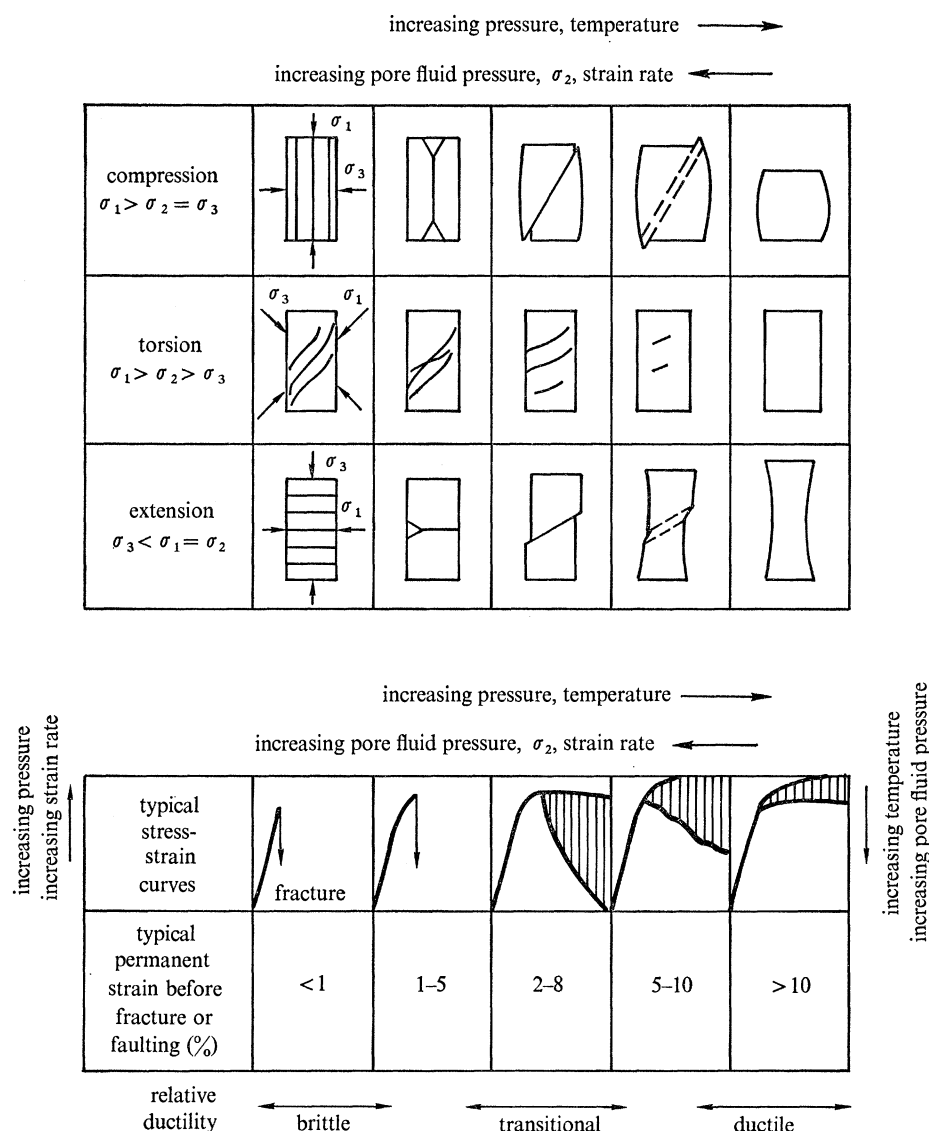

FIGURE 2. Schematic representation of transition in behaviour from brittle fracture to ductile flow for common loading states. Changing lithostatic or pore fluid pressure, σ_2, temperature, and strain rate shift the ductility and mechanical response horizontally. A change in lithostatic or pore fluid pressure, temperature, and strain rate will increase or decrease strength as shown on right or left sides. σ_2 may increase or decrease strength (Griggs & Handin 1960; Handin *et al.* 1967; Heard 1967).

differential stress–axial strain curve is shown at the bottom along with typical strains before fracture. As pressure and/or temperature are increased or pore pressure and/or strain rate are decreased, tensile fracture gives way to shear fracture or faulting (second, third and fourth column) and ultimately to homogeneous ductile flow (fifth column). The shape and position of the accompanying stress–strain curve (bottom) change markedly with physical conditions;

typical permanent strains of $< 1\%$ increase to $> 10\%$. At intermediate strains, the initial plastic flow in the component minerals occurs by dislocation motion and is accompanied by work hardening (primary creep). Further changes in the deformation environment leading to higher strains favour steady-state flow (secondary creep) by dislocation motion and/or diffusion of the mineral components (figure 2, right column). Permanent strains necessary to achieve steady-state flow vary from about 1% to somewhat greater than 10%, depending at least on the material, dislocation concentration, temperature and strain rate (Bird *et al.* 1969; Garofalo 1965). The resulting stress–strain curve approximates the shape characteristic of a model elastic-plastic material. Tertiary creep leading to fracture may or may not occur, depending on the imposed strain.

For other imposed stress fields (middle and lower rows, figure 2), the general behaviour of the material and its stress–strain curve are identical to that described above. However, an increase in the relative value of the intermediate principal stress (compared to that of the least stress) suppresses ductility if all other parameters are held constant (Handin *et al.* 1967). It may, however, either raise or lower the level of the stress–strain curve slightly, depending on the rock.

Field evidence demonstrates conclusively that brittle-transitional behaviour commonly occurs in many rocks in the upper crust. Griggs & Handin (1960) have discussed the influence of the deformation environment upon the fracture-faulting process and have emphasized the influence of rock properties on earthquake generation. Others have noted the influence of physical conditions on brittle behaviour occurring in many rocks in the crust (Hubbert & Rubey 1959; Heard & Rubey 1966; Stearns 1968). There also is abundant field evidence that all rocks can be highly deformed with little or no trace of fracture, given the appropriate tectonic regime. Although primary and tertiary creep may contribute locally to the observed natural deformations, any such large-scale strain in the crust must be attributed to secondary creep. The intention here is to consider only such flow, and thus the effective pressure (lithostatic pressure less pore pressure) need be only sufficient to inhibit fracture. Under these conditions, any effect from the intermediate stress can be expected to be negligible (Handin *et al.* 1967; Heard 1972). Our primary interest will be steady-state flow governed by the remaining environmental parameters: temperature, stress difference and strain rate. Depending on the rock type to be discussed as well as on the primary region of occurrence for that rock in the crust, reasonable bounds that have been placed on these parameters are: -30–$800\,°C$, $300\,MPa$–$100\,Pa$ and 10^{-7}–$10^{-15}\,s^{-1}$, respectively.

STRESS, TEMPERATURE AND STRAIN RATE-DEPENDENT FLOW IN THE CRUST

It is generally accepted that processes producing pure ductile flow (e.g. twinning, gliding, polygonization, recrystallization, volumetric diffusion or grain boundary slip) encompassing the primary and secondary stages of creep are governed by dislocation motion and/or diffusion, depending on the stress (σ), temperature (T) and strain rate ($\dot{\varepsilon}$) of deformation (Garofalo 1965). Tertiary or accelerating creep has been generally attributed to the opening of voids at grain triple-point junctions and leads to fracture. We will not consider it further here. Data on metals, ceramics and a limited number of minerals supporting this view are summarized and discussed by Sherby & Burke (1967), Bird *et al.* (1969), as well as Kirby & Raleigh (1973). When these materials are deformed at high stresses and at T/T_m greater than about 0.4, where

T_{m} is the melting temperature (K), dislocations multiply and move primarily on their glide plane in the appropriate direction. Diffusion of material components is not important in this case. The resultant dislocation interaction makes further straining more difficult and, hence, there is work hardening (primary creep). At higher temperatures and/or at somewhat lower stresses (and thus, lower strain rates), there is additional time for either the glide and climb of edge dislocations around pinning points or for the movement of jog-dragging screw dislocations. When the generation rate of dislocations by either process is equal to the annihilation rate by migration to the crystal boundary (subboundary) or by interaction with similar dislocations of opposite sign, steady-state flow or secondary creep results. Secondary creep by either mechanism commonly occurs at $\dot{\epsilon}/D < ca.$ 10^{-14} or at $\sigma/\mu < ca.$ 10^{-3}, where D is the diffusivity of the slowest moving component in the mineral and μ is the shear modulus for the aggregate (Sherby & Burke 1967; Weertman 1970; Kirby & Raleigh 1973). At still lower stresses, and usually near $\dot{\epsilon}/D \leqslant 10^2$, steady-state flow is still present but the mechanism responsible becomes solely diffusion, occurring either wholly within the grain or along grain boundaries (Nabarro 1948; Herring 1950; Coble 1963).

It has also been well documented that secondary creep is a thermally activated process. At the higher σ and $\dot{\epsilon}$, the empirically derived equation relating σ, T and $\dot{\epsilon}$ for most of the above materials is of the form

$$\dot{\epsilon} = A \exp\left(-Q/RT\right) \exp\left(B\sigma\right), \tag{1}$$

where A, B, and R are constants and Q is an activation energy for creep (Sherby & Burke 1967). For secondary creep with $10^9 > \dot{\epsilon}/D > 10^2$, most data are better fitted by

$$\dot{\epsilon} = A \exp\left(-Q/RT\right) \sigma^n \tag{2}$$

or

$$\dot{\epsilon} = A\left(\mu/T\right) \exp\left(-Q/RT\right) \left(\sigma/\mu\right)^n, \tag{3}$$

where the value of n ranges generally from 2 to 8. In equations (2) and (3), observed values of Q have been correlated with the activation energy for diffusion of the slowest moving component for many types of material (Sherby & Burke 1967). At $\dot{\epsilon}/D < 10^2$, n becomes 1 and the secondary creep data obey a theoretical equation of the type proposed by Nabarro (1948) and Herring (1950):

$$\dot{\epsilon} = A\sigma D_{\mathrm{v}}/l^2 T, \tag{4}$$

where D_{v} is the volume diffusivity and l is the average grain dimension. Some secondary creep data in this region also satisfy a relation suggested by Coble (1963):

$$\dot{\epsilon} = A\sigma D_{\mathrm{g}}/l^3 T, \tag{5}$$

where D_{g} is the grain boundary diffusivity.

Flow equations based on processes qualitatively similar to those encountered in secondary creep at high stress have been proposed by Kauzmann (1941) and by Ree et al. (1960). These equations are similar to (1) except the stress function $\exp\left(B\sigma\right)$ is replaced by $\sinh\left(B\sigma\right)$. When B is $\gg \sigma$, $\sinh\left(B\sigma\right) \simeq A \exp\left(B\sigma\right)$. Secondary creep equations of the form of (3) have been proposed by Weertman (1957, 1968) and by Barrett & Nix (1965), where n can range between 3 and 6, depending on the specific dislocation model assumed. Equation (3) often is simplified to (2), because of the lack of adequate data for μ. Use of equation (3) compared to (2) can give a slightly improved correlation of data for some metals and ceramics (see, for example, Bird et al. 1969). Where these two equations have been compared using data on geologic materials, no

statistical differences were found for either calcite (Heard & Raleigh 1972) or halite (Heard 1972). When observed, Nabarro–Herring or Coble flow described by equation (4) or (5) occurs in fine-grained aggregates at low stresses and usually at temperatures in excess of 0.8 T/T_m. If these restrictions carry over to minerals in the crust, then Nabarro–Herring or Coble creep could be expected only locally and not generally for most rocks at the conditions of interest here. The contribution to steady-state flow occurring by equation (1) or by $\dot{e} \propto \sinh (B\sigma)$ is probably not large if it exists at all.

We are left, then, with the probability that most large-scale, wholly ductile flow in the crust at intermediate to high temperatures is of the steady-state type and that we may describe it with sufficient accuracy by a power-law flow equation such as (2), with n generally between 2 and 8. It then follows that for this flow to dominate, the effective pressure need only be sufficient to inhibit fracture in any given rock over the range of temperatures, stresses and strain rates appropriate for natural deformation of that rock in the crust. Further, it is assumed for the purpose of this discussion that chemical effects (except those caused by trace amounts of bound H_2O in the component minerals) will not significantly alter the form of the steady-state flow equation or the values of the measured parameters from that equation. This latter assumption remains to be justified.

PREDICTED FLOW STRESSES AND EQUIVALENT VISCOSITIES IN THE CRUST

Only limited flow data are available for common rocks and minerals where steady-state flow at high temperatures can be demonstrated. These results for single-phase, polycrystalline rocks are summarized in table 1. Data on single crystals (e.g. olivine, halite) and on relatively uncommon geologic materials (e.g. periclase) have not been included. Also excluded are some data where values of the constants A, Q, and n from equation (2) could not be accurately characterized because of the limited range of experimental conditions or where fracture could not be excluded (e.g. limestone, marble, ice). The only known example of a polyphase rock, a peridotite composed of about two thirds olivine and one third enstatite-plus-diopsite, was not considered as the flow behaviour in the presence of H_2O is virtually identical to the wet dunite listed in table 1 (Carter & Ave'Lallemant, 1970) and to the more limited measurements on orthoenstatite (Raleigh *et al.* 1971).

Griggs & Blacic (1965) as well as Griggs (1967) demonstrated that trace amounts of OH^- occurring in the structure of several silicates, (e.g. quartz, olivine) in concentrations of 10^{-2}–10^{-4} H/Si, strongly influenced the stress-temperature-strain rate response. Most subsequent deformation studies on these silicates at high temperatures have been carried out in the presence of small amounts of H_2O at unknown but presumably low pressure (high effective pressures) or on material dried in the laboratory at temperatures < 100 °C. These correspond to the 'wet' and 'dry' designations, respectively, as listed in table 1. It has been presumed that the presence or absence of excess H_2O during these tests corresponds in some way to a high (10^{-2}–10^{-3}?) or to a low (10^{-4}–10^{-5}?) H/Si concentration in the structure, respectively. No rock listed has been analysed for OH^- concentration representative of the temperature and pressure during deformation. Further, only a few determinations have been made on OH^- concentrations from natural crystals. The presence of these small amounts of H_2O in contact with quartz and olivine in the rocks from table 1 appears to make important differences in the measured values for n but not for Q in the case of the quartzite. Comparison of the wet and the dry dunite

results indicates significant disagreement: n and Q may be different by a factor of nearly 2 or they may be little affected by the presence of H_2O. More work is needed to resolve this question.
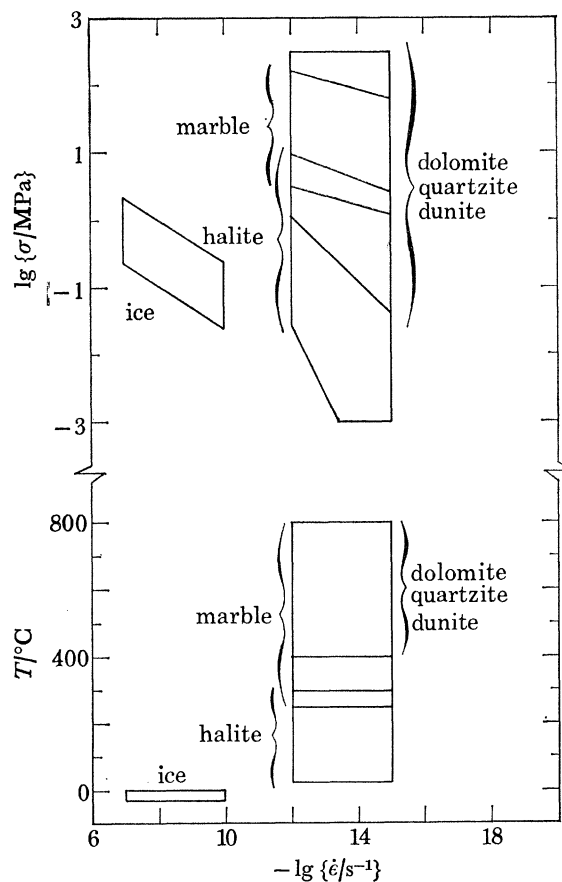

FIGURE 3. Expected range of steady-state flow stresses, temperatures and strain rates to be commonly encountered in the crust for the series of rocks indicated in table 1.

In direct contrast to the influence of H_2O on the mechanical behaviour of silicates, marble and limestone remain unaffected by H_2O (or CO_2) (Griggs *et al.* 1960; Heard 1960; Rutter 1974). In the latter work, Rutter was able to demonstrate that power-law creep according to equation (2) adequately describes both his dry as well as his wet data at 400–500 °C and that H_2O had a negligible effect on constants A, Q and n. In the case of halite, Carter & Heard (1970) reported trace mounts of H_2O exerted no influence on the behaviour of halite single crystals at high temperatures, although the few data are far from unequivocal. No data are available to assess the influence of H_2O on the flow behaviour of dolomite, but, judging from the calcite data, there probably is little if any effect.

The steady-state flow data for the rocks listed in table 1 may now be compared at lower stresses and crustal temperatures by solving equation (2) using the appropriate parametric values and extrapolating to the strain rate region of interest: $\dot{\epsilon} = 10^{-7}$–10^{-10} s^{-1} for ice and $\dot{\epsilon} = 10^{-12}$–$10^{-15}$ s^{-1} for all other rocks. In figure 3, the range of expected crustal stresses and temperatures are shown for these rocks at the appropriate strain rates. In the case of ice, the high and low stress limits are fixed by the -30–0 °C temperature range measured for polar and

temperate glaciers as well as by the A, Q and n values used with equation (2). For halite, the lower limit in temperature is taken as 25 °C (near-surface temperature); this then sets the upper bound for the expected stresses. Taking 300 °C to be the maximum temperature of interest for flowing halite in the crust, the lower limit of stress arbitrarily is truncated at 10^{-3} if Nabarro–Herring flow is operative. If power-law creep prevails here in halite, then the lower bounds on the stress will be somewhat higher. The maximum temperature of 800 °C taken for flow in all other rocks from table 1 controls the lower stress bounds for each individual rock in figure 3. The lower bounds are shown for marble and one set of data on wet dunite, the weakest of the silicates. The maximum stress assumed for flow in the crust, 300 MPa, limits the lower temperatures for steady-state flow for dolomite and all silicate rocks. The upper stress as well as the lower temperature boundary in marble is governed by the expected transition from steady-state flow to flow dominated by dislocation pile-up with consequent work hardening at about 250 °C (Heard & Raleigh 1972).
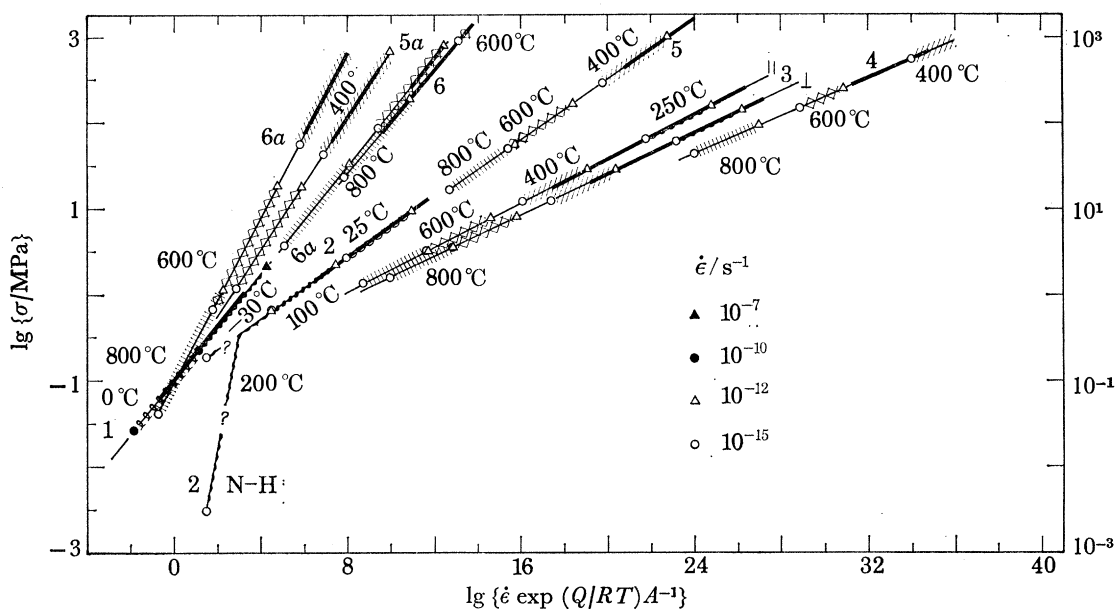

FIGURE 4. Log steady-state flow stress against a temperature, time compensated parameter $\lg [\dot{\epsilon} \exp (Q/RT)A^{-1}]$ for the rocks listed in table 1. Range of common crustal strain rates indicated at several temperatures for each rock. Accentuated line represents region of measured data. 1, ice; 2, halite; 3, marble $\perp$, $\parallel$; 4, dolomite; 5, quartzite; 5 a, quartzite, wet; 6, dunite; and 6 a, dunite, wet.

Within the temperature, stress, and strain-rate limits outlined above for the crust, the steady-state flow results for rocks listed in table 1 may be more easily compared graphically by solving equation (2) and plotting the value of the parameter $[\dot{\epsilon} \exp (Q/RT)A^{-1}]$ against σ on logarithmic scales as in figure 4. The choice of such a parameter for the abscissa allows regions of temperature and strain rate to be shown simultaneously. For each rock, the accentuated line corresponds to the region of measured data. The slope of each line is equal to n^{-1} for that rock; for halite at temperatures of 200 °C (and higher), the probable slope is 5.5^{-1} but if Nabarro–Herring creep occurs, the slope becomes unity. For the temperatures shown, the upper and lower values for the expected stresses correspond to the chosen limits of strain rate: 10^{-12}–10^{-15} s^{-1}, respectively, for each rock except ice. In that case, these bounds are 10^{-7}–10^{-10} s^{-1}. Comparisons of stress (and strain rate) between rocks may now be more easily accomplished at any

TABLE 1. SUMMARY OF AVAILABLE STEADY-STATE FLOW DATA FOR POLYCRYSTALLINE MONOMINERALIC ROCKS

Symbols ||, ⊥ indicate data for extension parallel and normal to the strong foliation, respectively. Possible Nabarro–Herring flow may occur in halite at $T > 200\ °C$. All data at one standard deviation.

$$\dot{\epsilon} = A \exp\left(-Q/RT\right)\sigma^n$$

| material	lg A (MPa^{-n} s^{-1})	$10^3\,Q$ cal mol^{-1}	n	reference
polycrystalline ice	20.6	31.8	3.2	Glen 1955
polycrystalline halite, dry	-0.1 ± 0.4	23.5 ± 0.9	5.5 ± 0.2	Heard 1972
Yule marble ⊥ ⎫ dry	-3.9 ± 0.4	62.0 ± 1.4	8.3 ± 0.2	Heard & Raleigh 1972
Yule marble || ⎭	-3.6 ± 0.4	60.7 ± 1.4	7.7 ± 0.2	
Crevola dolomite dry	-12.9 ± 2.6	83.2 ± 6.0	9.1 ± 0.9	Heard 1975 (unpublished)
Simpson quartzite dry	-10.1 ± 1.9	58.1 ± 5.0	5.7 ± 0.6	Heard & Carter 1968
Canyon Creek quartzite, wet	-1.4 ± 1.1	55.1 ± 6.7	2.6 ± 0.4	Parrish et al. 1975
Mt Burnet dunite, dry	3.1 ± 2.0	111.0 ± 14.0	3.3 ± 0.5	Carter & Ave'Lallemant 1970 (revised 1975)
Mt Burnet dunite, wet	-1.0 ± 0.7	54.0 ± 4.4	2.1 ± 0.2	Carter & Ave'Lallemant 1970 (revised 1975)
	2.2	93.1 ± 2.5	3.2 ± 0.2	Post & Griggs 1973
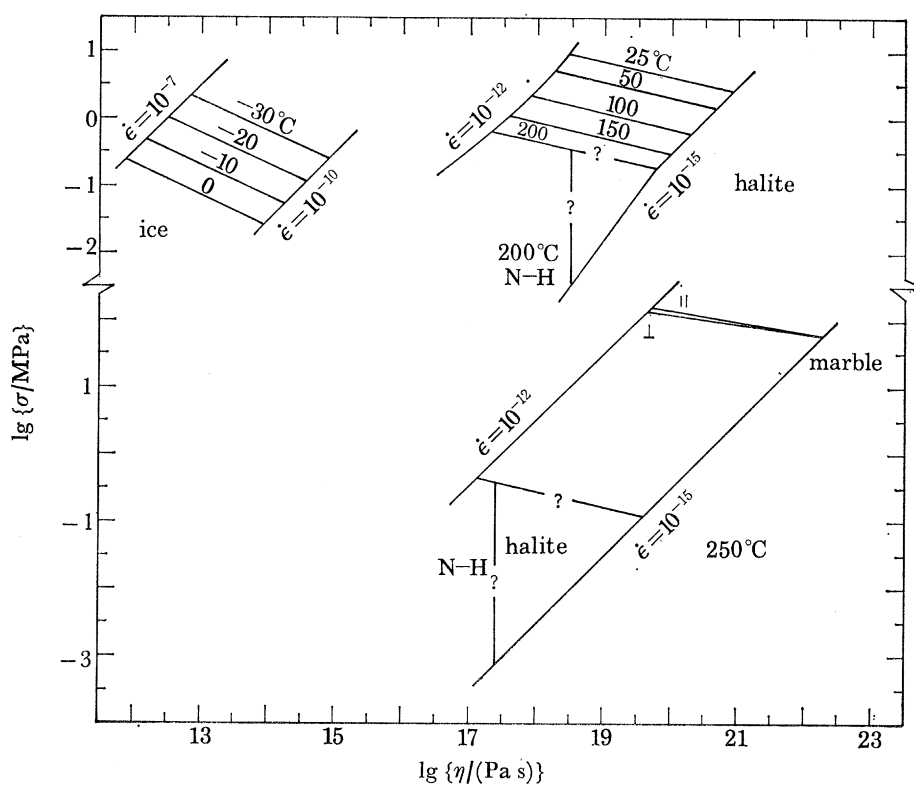
FIGURE 5. Log steady-state flow stress against log equivalent viscosity for ice, halite and marble. Temperatures indicated correspond to surface-to-intermediate depths, depending on rock type. Possible Nabarro–Herring flow region is indicated (N–H) at 200–250 °C for halite.

depth (temperature) chosen. As an example, considering the more intractable rocks at $\dot{\epsilon} = 10^{-15}\,\mathrm{s}^{-1}$ and at 400 °C, figure 4 shows dry dunite can be expected to be strongest followed by dolomite, dry quartzite, wet quartzite and marble. Placement of wet dunite in this progression is not possible at this time because of the disagreement among the input parameters (table 1) as mentioned above. At the same strain rate but at 800 °C, dolomite is strongest followed by dry dunite, dry quartzite, marble and wet quartzite. At relatively low temperatures of 250 °C, the expected strengths for halite are very much lower than for marble, regardless of power-law or Nabarro–Herring creep in the former.

The expected dependence of equivalent viscosity (η) on stress

$$\eta = \sigma/3\dot{\epsilon} \tag{6}$$

(Griggs 1939) as well as upon temperature is shown in figure 5 for the weaker rocks at the lower temperatures. For each rock type, the maximum and minimum values for η (and σ) along each isotherm are limited by the strain rates assumed to prevail during natural deformation. Thus, the calculated η for ice at glacier strain rates ranges from 8×10^{11} to 9×10^{13} Pa s at 0 °C and 7×10^{12} to 8×10^{14} Pa s at -30 °C (figure 5). These values are the lowest to be expected for any rock from table 1. Values of η characteristic of steady-state flow in massive halite bodies or in halite from folded evaporite sequences at strain rates of 10^{-12}–$10^{-15}\,\mathrm{s}^{-1}$ and a temperature of 25–300 °C may vary from 9×10^{20} to 3×10^{16} Pa s respectively. In this case, η seems relatively insensitive to temperature. If Nabarro–Herring creep is present at the higher temperatures, the viscosities would be Newtonian and dependent only upon temperature as shown in figure 5. At 250 °C (and at somewhat higher temperatures), if flow is assumed to be governed by equation (2), halite should exhibit η lower by a factor of 380–550 than for marble. However, if Newtonian behaviour exists in the halite, this ratio could approach 10^5 at 250 °C, $\dot{\epsilon} = 10^{-15}\,\mathrm{s}^{-1}$.

In figure 6, η and σ are similarly compared for marble and dolomite, as well as for the wet and dry quartzite and dunite at temperatures of 400–800 °C. Here at any $\dot{\epsilon}$, η of marble, dolomite and dry quartzite are only slightly influenced by temperature. However, expected η for wet quartzite, wet dunite and dry dunite may be lowered by 10^2–10^3 as temperature is increased by 400 °C. This η sensitivity to temperature is directly related to the form of the flow equation (2), the dependence of η on σ, $\dot{\epsilon}$ and the ratio of Q/n for each rock from table 1. In dry quartzite, dolomite, marble, halite and ice, Q/n is 4–10; in wet quartzite, as well as in wet and dry dunite, the ratio of Q/n ranges from 21 to 34.

At the strain rates and temperatures shown in figure 6, η is generally highest for dolomite followed by dry quartzite and marble, as might be expected from inspection of figure 4. At 400 °C at $\dot{\epsilon} = 10^{-15}\,\mathrm{s}^{-1}$, these values are 2×10^{23}, 10^{23} and 4×10^{21} Pa s, respectively; at 800 °C these values become 10^{22}, 6×10^{21} and 5×10^{20} Pa s, respectively. For wet quartzite at 400 °C, η is intermediate between dry quartzite and marble; at 800 °C it becomes more than an order of magnitude lower than for marble. In general, η for dry as well as wet dunite follow the above trends but because of the conflicting data shown in table 1, no direct comparison seems warranted at this time.

It is also useful to compare the expected flow behaviour for those rocks occurring in close proximity within folded or otherwise deformed sequences in the crust. At $\dot{\epsilon} = 3 \times 10^{-14}\,\mathrm{s}^{-1}$, σ and η for several rocks are normalized with respect to σ and η for marble and dolomite, and the normalized ratio of each parameter is plotted against temperature (figure 7). At intermediate-to-great depths (and hence, temperatures), the σ required to sustain steady-state flow

in dry quartzite can be expected to be about 30–15 times higher than for marble. Contrasts in η would be identical. However, σ and η for dry quartzite would be lower by a factor of only about 2 when compared to dolomite. Expected σ and η for dolomite thus would be 45–30 times those for marble at these depths. Comparison of similar properties for wet quartzite against either marble or dolomite shows a much greater depth (temperature) dependence. Figure 7 shows the σ and η of dolomite to be greater than that of wet quartzite by 5–140 between 400 and 800 °C, respectively. For wet quartzite compared to marble, these properties are greater by about 50 at 300 °C. At about 575 °C, these properties become equal; by 800 °C, wet quartzite would have only about one fifth the σ and η calculated for marble. At shallow-to-intermediate
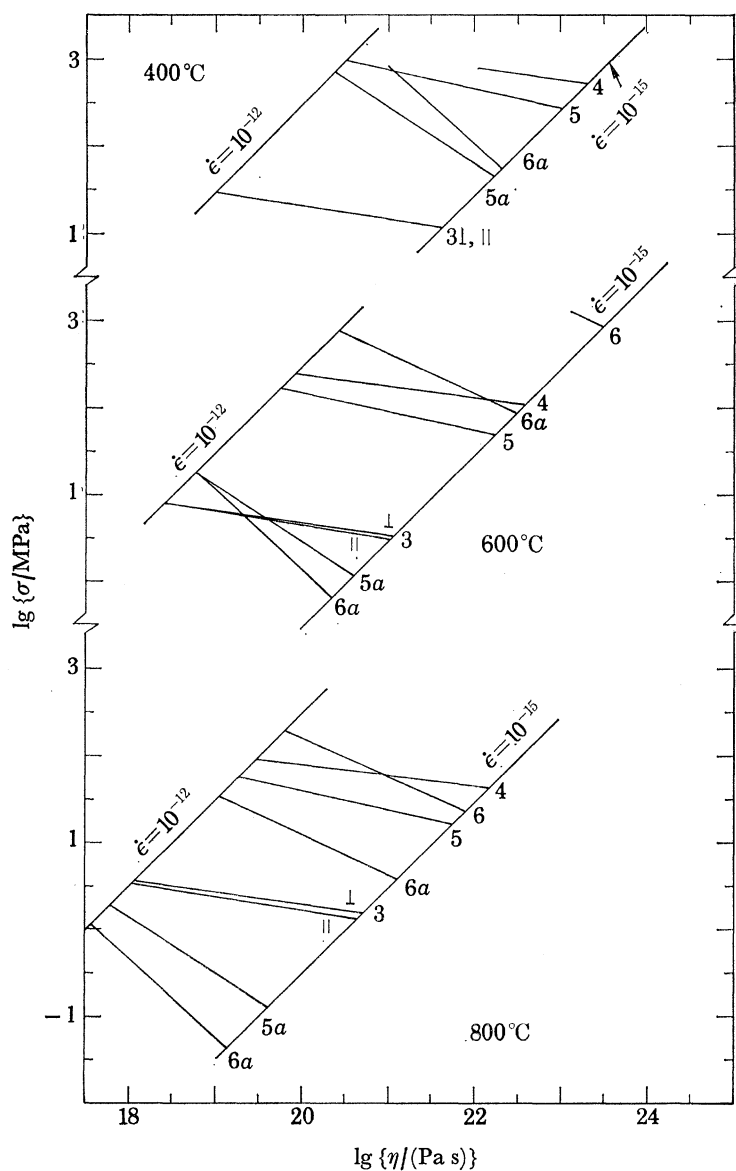

FIGURE 6. Log steady-state flow stress vs log equivalent viscosity for marble, dolomite, quartzite, and wet quartzite, dunite, and wet dunite at 400–800 °C. Numbers refer to: 3, marble $\perp$, $\parallel$; 4, dolomite; 5, quartzite; 5a, quartzite, wet; 6, dunite; and 6a, dunite, wet.

depths (250–300 °C in figure 7), halite would be weaker and possess a lower equivalent viscosity than marble by a factor of 300–400. If Nabarro–Herring flow occurs, then these contrasts may range from 10^4 to 10^5.

It should be emphasized to the user of data such as these, that, with the exception of ice, the rheological behaviour predicted here lies far outside the range of accessible measurement. All inferences as to σ and η to be expected at geologic strain rates are strongly influenced not only by the form of the flow equation chosen but also by the assumption that the constants in those equations determined at high σ, T and $\dot{\epsilon}$ in the laboratory do not change at the low σ and $\dot{\epsilon}$ characteristic of natural flow in the crust. However, the equivalence of the deformation mechanisms producing flow in nature with those occurring during laboratory deformation for the same mineral taken together with the well-characterized mechanical behaviour and a reasonable theoretical basis for that behaviour, strongly suggest that the steady-state flow properties inferred here for natural deformation in the crust are valid.
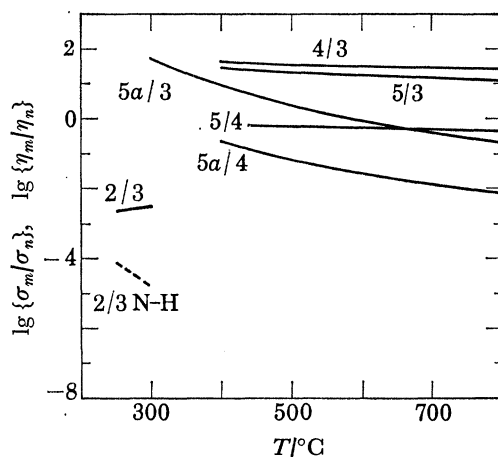

FIGURE 7. Normalized steady-state flow stress and equivalent viscosity against temperature for halite, marble, dolomite, quartzite and wet quartzite. Numerator and denominator in fraction refer to rock type. N–H indicates constrast if Nabarro–Herring flow occurs in halite. $m, n = 2$, halite; 3, marble ($\perp$); 4, dolomite; 5, quartzite; 5a, quartzite (wet).

REFERENCES (Heard)

Barrett, C. R. & Nix, W. D. 1965 *Acta. Metall.* **13**, 1247.
Birch, F. 1964 *State of stress in the Earth's crust* (ed. W. R. Judd), p. 55. New York: American Elsevier.
Bird, J. E., Mukherjee, A. K. & Dorn, J. F. 1969 *Quantitative relation between properties and microstructure*, p. 255. Jerusalem: Israel University Press.
Bridgeman, P. W. 1945 *Am. J. Sci.* **243a**, 90.
Carter, N. L. & Ave'Lallemant, H. G. 1970 *Geol. Soc. Am. Bull.* **81**, 2181.
Carter, N. L. & Heard, H. C. 1970 *Am. J. Sci.* **269**, 193.
Coble, R. L. 1963 *J. appl. Phys.* **34**, 1679.
Crittenden, M. D. Jr. 1967 *Geophys. J. R. astr. Soc.* **14**, 261.
Dickinson, G. 1953 *Am. Ass. Petrol Geol. Bull.* **37**, 410.
Garofalo, R. 1965 *Fundamentals of creep and creep rupture in metals.* New York: Macmillan.
Gerrard, J. A. F., Perutz, M. F. & Roch, A. 1952 *Proc. R. Soc. Lond.* A **213**, 546.
Gilluly, J. 1972 *The Nature of the solid Earth* (ed. E. E. Robertson), p. 406. New York: McGraw-Hill.
Glen, J. W. 1955 *Proc. R. Soc. Lond.* A **228**, 519.
Gow, A. J., Ueda, H. T. & Garfield, D. E. 1968 *Science, N.Y.* **161**, 1011.

Gretener, P. E. 1967 *Geophysics* **32**, 727.

Griggs, D. T. 1939 *J. Geol.* **3**, 255.

Griggs, D. T. 1940 *Geol. Soc. Am. Bull.* **51**, 1001.

Griggs, D. T. 1967 *Geophys. J. R. astr. Soc.* **14**, 19.

Griggs, D. T. & Blacic, J. D. 1965 *Science, N.Y.* **147**, 292.

Griggs, D. T. & Handin, J. 1960 *Rock deformation* (ed. D. T. Griggs & J. Handin), p. 347. *Geol. Soc. Am. Mem.* **79**.

Griggs, D. T., Turner, F. J. & Heard, H. C. 1960 *Rock deformation* (ed. D. T. Griggs & J. Handin), p. 39. *Geol. Soc. Am. Mem.* **79**.

Handin, J., Heard, H. C. & Magouirk, J. N. 1967 *J. geophys. Res.* **72**, 611.

Heard, H. C. 1960 *Rock deformation* (eds. D. T. Griggs & J. Handin), p. 139. *Geol. Soc. Am. Mem.* **79**.

Heard, H. C. 1967 *Failure and breakage of rock* (ed. C. Fairhurst), p. 82. New York: AIME.

Heard, H. C. 1972 *Flow and fracture of rocks* (ed. H. C. Heard, I. Y. Borg, N. L. Carter & C. B. Raleigh), p. 191. *Am. Geophys. Union Monogr.* **16**.

Heard, H. C. & Carter, N. L. 1968 *Am. J. Sci.* **266**, 1.

Heard, H. C. & Raleigh, C. B. 1972 *Geol. Soc. Am. Bull.* **83**, 935.

Heard, H. C. & Rubey, W. W. 1966 *Geol. Soc. Am. Bull.* **77**, 741.

Heirtzler, J. R., Dickson, G. O., Herron, E. M., Pitman, W. C. III & Le Pichon, X. 1968 *J. geophys. Res.* **73**, 2119.

Herrin, E. 1972 *The nature of the solid Earth* (ed. E. C. Robertson), p. 216. New York: McGraw-Hill.

Herring, C. 1950 *J. appl. Phys.* **21**, 437.

Hubbert, M. K. & Rubey, W. W. 1959 *Geol. Soc. Am. Bull.* **70**, 115.

Jeffreys, H. 1970 *The Earth.* Cambridge University Press.

Kamb, B. 1964 *Science, N.Y.* **146**, 353.

Kauzmann, W. 1941 Tech. paper 1301 in *AIME* **8**, 25.

Kirby, S. H. & Raleigh, C. B. 1973 *Tectonophysics* **19**, 165.

Lachenbruch, A. H. 1968 *J. geophys. Res.* **73**, 6977.

Le Pichon, X. 1973 *J. geophys. Res.* **73**, 3661.

Meier, M. F. 1960 *U.S. Geol. Surv. Prof. Pap.* **351**.

Moses, P. L. 1961 *World Oil* **152**, 79.

Nabarro, F. R. N. 1948 *Strength of solids*, p. 175. Section of the *AIME*. London: The Physical Society.

Nichols, E. A. 1947 *Petrol. Dev. Tech. Trans., AIME* **170**, 44.

Parrish, D. K., Kriva, A. & Carter, N. L. 1975 *Geol. Soc. Am. Bull.* (In the Presss.)

Paterson, W. S. B. & Savage, J. C. 1963 *J. geophys. Res.* **68**, 4521.

Post, R. L., Jr & Griggs, D. T. 1973 *Science, N.Y.* **181**, 1242.

Raleigh, C. B., Kirby, S. H., Carter, N. L. & Ave'Lallemant, H. G. 1971 *J. geophys. Res.* **76**, 4011.

Ree, F. H., Ree, T. & Eyring, H. 1960 *J. Eng. Mech. Div., Am. Soc. Civil Eng. Proc.* **86**, 41.

Rubey, W. W. & Hubbert, M. K. 1959 *Geol. Soc. Am. Bull.* **70**, 167.

Rutter, E. H. 1974 *Tectonophysics* **22**, 311.

Sherby, O. D. & Burke, P. M. 1967 *Progr. Mater. Sci.* **13**, 325.

Stearns, D. W. 1968 *Kink bands and brittle deformation* (ed. A. J. Baer & D. K. Norris), p. 79. *Geol. Soc. Can. Pap.* 68–52.

Weertman, J. 1957 *J. appl. Phys.* **28**, 362.

Weertman, J. 1968 *Am. Soc. Metals. Trans.* **61**, 681.

Weertman, J. 1970 *Rev. Geophys. Space Phys.* **8**, 145.

Whitten, C. A. 1956 *Am. Geophys. Union Trans.* **37**, 393.